Biomedicine & Pharmacotherapy 107 (2018) 1302–1310

Contents lists available at ScienceDirect

Biomedicine & Pharmacotherapy

journal homepage: www.elsevier.com/locate/biopha

Synthesis and evaluation of thiazolidine-2,4-dione/benzazole derivatives as inhibitors of protein tyrosine phosphatase 1B (PTP-1B): Antihyperglycemic activity with molecular docking study

Sergio Hidalgo-Figueroa[a,*,1], Samuel Estrada-Soto[b], Juan José Ramírez-Espinosa[b], Paolo Paoli[c], Giulia Lori[c], Ismael León-Rivera[d], Gabriel Navarrete-Vázquez[b,**]

[a] CONACyT, IPICYT/ Consorcio de Investigación, Innovación y Desarrollo para las Zonas Áridas, Camino a la presa San José 2055, Lomas 4a secc., San Luis Potosí, 78216, Mexico
[b] Facultad de Farmacia, Universidad Autónoma del Estado de Morelos, Cuernavaca, Morelos, Mexico
[c] Department of Experimental and Clinical Biomedical Sciences "Mario Serio", Florence, Italy
[d] Centro de Investigaciones Químicas, IICBA, UAEM, Cuernavaca, Morelos, Mexico

ARTICLE INFO

Keywords:
Thiazolidine-2,4-dione
Antihyperglycemic
Molecular docking
PTP-1B

ABSTRACT

This work presents the synthesis of two hybrid compounds (**1** and **2**) with thiazolidine-2,4-dione structure as a central scaffold which were further screened *in combo* (*in vitro* as PTP-1B inhibitors, *in vivo* antihyperglycemic activity, *in silico* toxicological profile and molecular docking). Compound **1** was tested in the enzymatic assay showing an IC_{50} = 9.6 ± 0.5 μM and compound **2** showed about a 50% of inhibition of PTP-1B at 20 μM. Therefore, compound **1** was chosen to test its antihyperglycemic effect in a rat model for non-insulin-dependent diabetes mellitus (NIDDM), which was determined at 50 mg/kg in a single dose. The results indicated that compound showed a significant decrease of plasma glucose levels that reached 34%, after a 7 h post-administration. Molecular docking was employed to study the inhibitory properties of thiazolidine-2,4-dione derivatives against Protein Tyrosine Phosphatase 1B (PDB ID: 1c83). Concerning to the two binding sites in this enzyme (sites A and B), compound **1** has shown the best docking score, which indicates the highest affinity. Finally, compounds **1** and **2** have demonstrated an in silico satisfactory pharmacokinetic profile. This shows that it could be a very good candidate or leader for new series of compounds with this central scaffold.

1. Introduction

Thiazolidinone and thiazolidine-2,4-dione (glitazone) are important nucleus of heterocyclic bioactive compounds that have several different biological properties such as anti-tumor [1–3], anti-inflammatory [4–6], antimicrobial [7–10], antiviral [11,12], anticonvulsant [13,14], antifungal [15], tyrosinase inhibitor [16] and antidiabetic activities [17,18].

Moreover, glitazone drugs such as pioglitazone and rosiglitazone (PPARγ agonists) also containthiazolidine-2,4-dione core and they are used for the treatment of diabetes mellitus type 2. Currently, this scaffold has encouraged the attention of two research groups [19–23] in their search for antidiabetic molecules through inhibition of Protein-tyrosine phosphatase 1B (PTP-1B). This enzyme is a promising target for the diabetes treatment, and it has been implicated as a negative regulator of insulin-stimulated pathways [24–28].

PTP-1B has a catalytic site where the negatively charged phosphate of tyrosine is recognized, then it is hydrolyzed by a catalytic triad that is composed of Asp181, Cys215, Arg221 residues [29] and the phenyl ring of phosphotyrosine is stabilized by Tyr 46 and Phe182 [29,30]. Hence, lies the importance of knowing the involvement of these residues in ligand recognition to facilitate the design of new drug candidates due to their pharmacological resistance in a chronic degenerative disease such as diabetes. In order to obtain new ligands with affinity and selective recognition to PTP-1B, our research group has designed and synthesized the two compounds (**1** and **2**) with phenol moiety (tyrosine-like fragment) and thiazolidine-2,4-dione as a central scaffold. Finally, it has used the aza/thiaza heterocyclic portion in order to test them *in vitro*

* Corresponding author at: Cátedra CONACyT, IPICYT/ Consorcio de Investigación, Innovación y Desarrollo para las Zonas Áridas, Camino a la Presa San José 2055, Lomas 4a secc., San Luis Potosí, 78216, Mexico.
** Corresponding author at: Facultad de Farmacia, UAEM, Cuernavaca, Morelos, Mexico.
E-mail addresses: sergio.hidalgo@ipicyt.edu.mx (S. Hidalgo-Figueroa), gabriel_navarrete@uaem.mx (G. Navarrete-Vázquez).
[1] Taken in part from the Ph.D. Thesis of S. Hidalgo-Figueroa.

https://doi.org/10.1016/j.biopha.2018.08.124
Received 13 April 2018; Received in revised form 18 August 2018; Accepted 23 August 2018

inhibition of PTP-1B, as well as the *in vivo* antidiabetic effect of each compound.

2. Material and methods

2.1. Chemistry

Commercially obtained chemicals and solvents were used without further purification. First, all the round-bottom flasks were dried. Second, the melting points were taken in open glass capillaries using the EZ-Melt MPA120 automated melting point apparatus from Stanford Research Systems. Then, the reactions were monitored by TLC on 0.2 mm precoated Silica Gel 60 F254 plates (E. Merck). ^{1}H and ^{13}C NMR spectra were recorded by using a Varian Inova 400 MHz (9.4 T) NMR spectrometer. Next, the chemical shifts were given at ppm relative to tetramethylsilane (TMS), and samples were dissolved in DMSO-d_6. Last, the Chemical Ionization (CI) and positive Fast Atom Bombardment (FAB+) mass spectra (mNBA matrix), were recorded on a JEOL JMS-SX102 A spectrum.

2.1.1. N-(1,3-benzo[d]thiazol-2-yl)-2-[(5Z)-5-(4-hydroxybenzylidene)-2,4-dioxo-1,3-thiazolidin-3-yl]acetamide (1)

A solution of (*Z*)-5-(4-hydroxybenzylidene)-1,3-thiazolidine-2,4-dione **3** (0.3 g, 1.3 mmol) and K_2CO_3 (0.2 g, 1.5 mmol) was dissolved in 10 mL of dimethylformamide in a round bottom flask with a magnetic stirrer. Then, the *N*-(benzo[*d*]thiazol-2-yl)-2-chloroacetamide **5** (6.7 mmol) were added and stirred at room temperature (25 °C) during 4 days. Once the reaction was completed, the mixture was poured into water and the resulting precipitate was filtered. The product was purified through the column chromatography (mixture of eluents: CH_2Cl_2-AcOEt in 80:20 ratio). Finally, it was dried under vacuum to give 0.31 g of a yellow compound (yield 56%). Mp: 235.6–236.8 °C. ^{1}H NMR (400 MHz, DMSO-d_6) δ: 2.67 (s, 2H, CH_2), 5.11 (s, OH), 6.75 (d, 2H, H-4, H-7, *Jo* = 8.4 Hz), 6.85 (d, 2H, H-5, H-6, *Jo* = 8.4 Hz), 6.97 (s, 1H, HC = C), 7.90(s, 1H, NH-C = O), 7.30 (d, 2H, H-3´, H-5´, *Jo* = 8 Hz), 7.44 (d, 2H, H-2´, H-6´, *Jo* = 8 Hz), ^{13}C NMR (100 MHz, DMSO-*d6*) δ: 67.66 (NCH2-), 116.56 (C-4, C-7), 121.82 (C-5, C-6), 123.84 (C-3´, C-5´), 126.17(C-2´), 126.31(C-6´), 132.86 (C-2), 148.44(O = C-C = *C*), 151.12 (O = C-*C* = C), 165.90 (= C*C* = *O*N), 167.63 (CH_2*C* = *O*N), 175.12 (S*C* = *O*N). MS (Cl+) *m/z* 412 (M^+, 5).

2.1.2. (5Z)-3-(1H-benzo[d]imidazol-2-ylmethyl)-5-(4-hydroxybenzylidene)-1,3-thiazolidine-2,4-dione (2)

The solution was placed in a round-bottom flask containing a magnetic stirrer, with (*Z*)-5-(4-hydroxybenzylidene)-1,3-thiazolidine-2,4-dione **3** (0.2 g, 0.9 mmol) and K_2CO_3 (0.13 g, 1.1 mmol) it was dissolved in 2 mL of dimethylformamide. Fifteen minutes after the dissolution, 2-(chloromethyl)-1H-benzo[*d*]imidazole **4** (0.15 g, 0.9 mmol) were added and stirred at room temperature (25 °C) for 12 h. Once the reaction was complete, the mixture was poured into water and the resulting precipitate was filtered. The product was purified by a chromatography column (mixture of eluents CH_2Cl_2-AcOEt in 80:20 ratios). The obtained product was dried under vacuum to give a yellow compound with a yield of 0.15 g. Yield 55%. Mp: 214–215.5 °C. ^{1}H NMR (400 MHz, DMSO-d_6) δ: 3.32 (s, CH_2), 5.27(s, NH), 5.73(s, O-H), 6.92(d, 2H, H-2, H-6, *Jo* = 8. 6 Hz), 7.09-7.20(m, 2H, H-5´, H-6´, *Jm* = 3 Hz, *Jm* = 3.2 Hz, *Jo* = 6.2 Hz, *Jo* = 7 Hz), 7.46–7.53 (m, 4H, H-3, H-5, H-4´, H-7´, *Jm* = 3 Hz, *Jo* = 5.0 Hz, *Jo* = 8.6 Hz), 7.89 (s, H-7) ppm. ^{13}C NMR (100 MHz, DMSO-*d6*) δ: 116.84(C-4´, C-7´), 117.01(C-2, C-6), 124.07(C-5´, C-6´), 133.17(C-3, C-5), 149.13(C-7), 161.08(*C*-OH), 165.92(= C*C* = *O*N), 167.80(S*C* = *O*N) ppm. MS (Cl+) *m/z* 351 (M^+, 5).

2.1.3. N-(benzo[d]thiazol-2-yl)-2-chloroacetamide (5)

A solution of 2-aminobenzothiazole (1.0 g, 6.6 mmol) and triethylamine (0.67 g, 0.93 mL, 6.7 mmol) was dissolved in 10 mL of dichloromethane in the round bottom flask equipped with a magnetic stirrer and ice bath. After fifteen minutes, 2-chloroacetyl chloride (6.7 mmol) were slowly added and stirred at room temperature (25 °C) for 2 h. Once the reaction was completed, a solvent was filtered and then evaporated *in vacuum* to give a pure compound (white solid) with a yield of 1.05 g (yield 72%). Mp: 135–137 °C. ^{1}H NMR (400 MHz, DMSO-d_6) δ: 4.21(s, 2H, CH_2-Cl), 7.53(m, 2H, H-5, H-6), 8.01(m, 1H, H-7), 8.18(m, 1H, H-4) ppm. ^{13}C NMR (100 MHz, DMSO-*d6*) δ: 42.7(CH_2-Cl), 118.31(C-4), 121.16(C-7), 124.5(C-6), 125.35(C-5), 168.65 (C = O) ppm.

2.1.4. (Z)-5-(4-hydroxybenzylidene)-1,3-thiazolidine-2,4-dione (3)

In a round bottom flask with a magnetic stirrer, the solution of thiazolidine-2,4-dione **7** (0.959 g, 8.2 mmol), *p*-hydroxybenzaldehyde **6** (1 g, 8.1 mmol) and benzoic acid (0.3 g, 2.5 mmol) in toluene (10 mL) was heated at 40 °C until complete dissolution. Under these conditions and showing a translucent solution, the piperidine (0.242 mL, 2.5 mmol) was immediately added and the reaction mixture was refluxed for 6 h with the Dean-Stark apparatus. Once the reaction had been completed, the mixture was filtered, and the filtered solution was concentrated under vacuum. The yellow precipitate was washed with cold toluene and acetone to obtain a pure solid with a yield of 1.77 g (yield 94%). Mp: Dec 200 °C, ^{1}H NMR (400 MHz, DMSO-d_6) δ: 6.9 (d, 2H, H-2, H-6, *Jo* = 8.55 Hz), 7.43 (d, 2H, H-3, H-5, *Jo* = 8.55 Hz), 7.64 (s, 1H, H-7). ^{13}C NMR (100 MHz, DMSO-*d6*) δ: 116.22(C-2, C-6), 120.29(C-4), 124.16(C- 8), 131.38(C-7), 132.16(C-3, C-5), 159.55 (C-1), 168.85 (C = O), 169.03 (C = O). MS (FAB^+) *m/z* 221 (M^+, 10).

2.2. In vitro studies

2.2.1. Enzyme section

The complete coding sequence of PTP1B was cloned in frame with the sequence of the glutathione S-transferase (GST) in the pGEX-2 T bacterial expression vector. The enzyme expression and purification were achieved in the *Escherichia coli* TB1 strain. Briefly, the recombinant fusion proteins were purified from bacterial lysate using a single step affinity chromatography of glutathione-Sepharose. The solution contained purified fusion proteins that were treated with thrombin for 3 h at 37 °C. Then the enzymes were purified from GST and thrombin by gel filtration on Superdex G-75. The purity of protein preparations was analyzed by SDS–polyacrylamide gel electrophoresis according to Laemmli [31].

2.2.2. Phosphatase assay and inhibition experiments

The phosphatase assay was carried out at 37 °C using *p*-nitrophenylphosphate as substrate; the final volume of each test was 1 mL. The assay buffer (pH 7.0) contained 0.075 M of β,β-dimethylglutarate buffer, 1 mM EDTA and 5 mM dithiothreitol. Furthermore, the reactions were initiated by adding the aliquots of the enzyme preparation and pausing at appropriate times by adding 4 mL of 1 M KOH. The amount of *p*-nitrophenolate ion release was determined by reading the absorbance of samples at 400 nm (e = 18,000 $M^{-1}\,cm^{-1}$). For each inhibitor, the IC_{50} value was determined by measuring the initial hydrolysis rate under a fixed *p*-nitrophenylphosphate concentration, which was equivalent to the *K*m value of the considered PTP, in the presence of increasing inhibitor concentrations. The obtained data were adjusted to the following equations using the Fig-Sys program:

$$y = \frac{Max - Min}{1 + \left(\frac{x}{IC_{50}}\right)^{slope}} + Min$$

were y = Vi/ V0, represent the ratio between the activity measuredin the presence of the inhibitor (Vi) and the activity of enzyme measured in the absence of the inhibitor (V0), while the parameter "x" represents the concentration of the inhibitor [32].

The main kinetic parameters (Km and Vmax) were determined by measuring the initial rates at different substrate concentrations. All experimental data were analyzed using the Michaelis-Menten equation and a non-linear fitting program (Fig-Sys). Inhibition constants were determined measuring initial hydrolysis rates at differing substrate and inhibitor concentrations. In order to determine the inhibition mechanism of compounds, the experimental data were analyzed using the double reciprocal plot method. *K*i values were determined using appropriate equations, depending on the inhibition mechanism of compounds. All the initial rate measurements were carried out in triplicate.

2.3. In vivo studies

2.3.1. Animals

Male Wistar rats weighing 200–250 g, were housed in standard laboratory conditions and fed with a rodent pellet diet and water ad libitum. They were maintained at room temperature and at a photoperiod of 12 h day/night cycle. Animals described as fasted had been deprived of food for 16 h., but had free access to tap water. All experimental animal procedures were carried out in conformity with the guidelines of our Federal Regulations for Animal Experimentation and Care (SAGARPA, NOM-062-ZOO-1999, México) and approved by the Institutional Animal Care and Use Committees funded by the US National Institutes of Health. (Publication number: 85-23, revised 1985).

2.3.2. Induction of diabetes

Streptozotocin (STZ) was dissolved in citrate buffer (pH 4.5) and nicotinamide in a normal physiological saline solution. The non-insulin-dependent diabetes mellitus rat model was induced in overnight fasted rats by a single intraperitoneal injection of 65 mg/kg STZ, 15 min after the i.p. administration of 110 mg/kg of nicotinamide. Hyperglycemia was confirmed by the elevated glucose concentration in plasma, determined at 72 h by a glucometer. The animals with the highest blood glucose concentrations of 250 mg/dL were used for the antidiabetic screening [17,33,34].

2.3.3. Non-insulin dependent diabetes mellitus rat model

The diabetic animals were divided into three groups of five animals each (n = 5). The experimental group rats were administered with a solution of compound **1** (50 mg/kg body weight, prepared with tween 80, 10%). In contrast, the animals in the control group were also treated with a saline plus tween 80, 10%. Additionally, Glibenclamide (5 mg/kg) was used as a hypoglycemic reference drug. Blood samples were collected from the caudal vein at 0, 1, 3, 5 and 7 h after vehicle, compound and drug administration. Then, the blood glucose concentration was estimated by an enzymatic glucose oxidase method using a commercial glucometer. The percentage variation of glycemia for each group was calculated in relation to an initial (0 h) level, according to:

$$\%\,\text{variation of glycemia} = \left(\frac{\text{GluX-Glu0}}{\text{Glu0}}\right)\times 100$$

where Glu0 were the initial glycemia values and GluX were the glycemia values at 1, 3, 5 and 7 h, respectively. All values were expressed as the mean ± S.E.M. Last, the statistical significance was estimated by an analysis of variance (ANOVA), where $p < 0.05$ implies significance.

2.4. In silico studies

2.4.1. Preparation of ligands

The three dimensional structures of each compounds were prepared using the Avogadro (http://avogadro.cc/) which minimized the ligand using a MMFF94 force field of steepest descent algorithms. The final configuration was saved as a.pdb file format [35–38]. These. pdb files were subjected to the AutoDock tool to prepare a. pdbqt file of each compound for molecular docking studies.

2.4.2. Molecular docking studies

The protein tyrosine phosphatase 1B was retrieved from the RCSB Protein Data Bank (http://www.rcsb.org/pdb/home/home.do/) as a PDB file with the access code: 1C83 (1.8 Å resolution) co-crystalized with 6-(oxalyl-amino)-1*H*-indole-5-carboxylic acid.

Then, a molecular docking was carried out using AutoDock4.2 and AutoGrid 1.5.3 [35]. The AutoDock had been performed with an automated docking of the ligand with a user-specified dihedral flexibility in a rigid protein binding site and the program performed several runs in each docking experiment. Each run provided one predicted binding mode. All water molecules and 6-(oxalyl-amino)-1*H*-indole-5-carboxylic acid (crystallographic ligand) were removed from the crystallographic structures, and all the hydrogen atoms were added. Additionally, all the ligands and proteins, gasteiger charges were assigned and non-polar hydrogen atoms were merged. Consequently, all the torsions were allowed to rotate during docking. The auxiliary program AutoGrid generated the grid maps. Each grid was centered at the crystallographic point coordinates of the crystallographic compound. The molecular docking protocol was carried out covering two binding sites (site A and site B). The grid dimensions were 60 × 60 × 60 points separated by 0.375 Å. The grid was generated by overlapping the residues of the catalytic and binding sites (Site A) such as Asp181, Cys215, Arg221 and other residues like Lys120, Ser216, Phe182, Gly220) and also covering Site B with the following residues: Arg24, Tyr46, Asp48, Val49, Ile219, Arg254, Met258 and Gln262 [42]. The Lamarckian genetic algorithm was applied to the search by using default parameters. The number of docking runs was 100. After the docking solutions had been clustered into groups of RMSD lower than 2.0 Å. The clusters were finally ranked by the lowest energy representative for each cluster.

2.4.3. Validation

Validation was performed in AutoDock 4.2 using crystal structure of protein tyrosine phosphatase 1B (PDB ID: 1C83). The X-ray crystal structure (6-(oxalyl-amino)-1*H*-indole-5-carboxylic acid) was built and docked overlying two binding site regions. The docking protocol was validated by re-docking co-crystal ligand (6-(oxalyl-amino)-1*H*-indole-5-carboxylic acid) comprising two active sites (A and B), the binding mode and site is the same as the co-crystal ligand. After the re-docking, we found that the root mean square deviation (RMSD) between the co-crystal ligand and the re-docked structure was 0.33 Å indicating that the parameters for docking simulations are good for orientation reproduction, conformation and interactions in the original x-ray crystal structure.

2.5. Pharmacokinetic profile

The Pharmacokinetic parameters were predicted for the synthesized compounds with the help of admetSAR tool (http://lmmd.ecust.edu.cn/admetsar2).

3. Results and discussion

3.1. Chemistry

The synthesis of two thiazolidine-2,4-dione derivatives (**1** and **2**) starting from intermediate compounds **3** and **5** to later convergent synthesis with the aim to improve their efficiency and yields. First, the acylation of 2-aminobenzothiazole (**9**) was carried out with 2-chloroacetyl chloride (**8**) giving corresponding compound **5** in reasonably good yields. On the other hand, to obtain the second most important moiety, *p*-hydroxybenzaldehyde (**6**) and thiazolidine-2,4-dione (**7**) were subjected to Knoevenagel conditions to obtain the required (Z)-5-

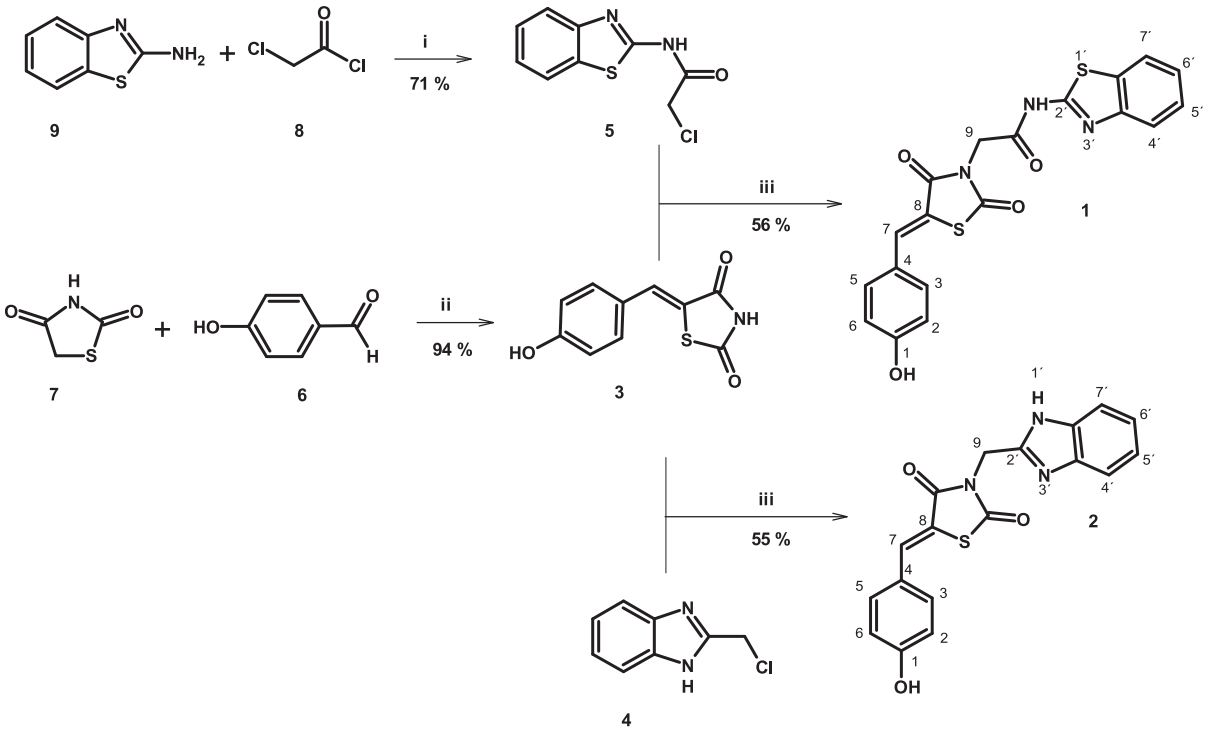

Scheme 1. Synthesis of thiazolidine-2,4-dione derivatives, conditions and reagents: i) Et_3N, CH_2Cl_2, r.t.; ii) Piperidine, benzoic acid, toluene, reflux; iii) K_2CO_3, DMF, r.t.

(4-hydroxybenzylidene)-1,3-thiazolidine-2,4-dione (**3**). Subsequently, the two moieties were used to a convergent synthesis where compounds **3** and **5** were treated under basic conditions at room temperature giving compound **1** in moderate yield (Scheme 1). For comparison purposes, the length of compound **1** was reduced by removing the amidic group spacer to find more details of the molecular requirements like flexibility. Therefore, heterocyclic moiety (benzimidazole) in compound **2** is only linked by a methylene group. In order to obtain the second final compound, (Z)-5-(4-hydroxybenzylidene)-1,3-thiazolidine-2,4-dione (**3**) and 2-chloromethylbenzimidazole (**4**) were subjected to an SN^2 reaction. The final compounds were recovered with moderate yields (± 50%) and were characterized by a ^1H, ^{13}C-Nuclear Magnetic Resonance and Mass Spectral Analysis. ^1H-NMR spectra of the compounds **1** and **2** showed a typical proton to methine signal at 7.68 ppm corresponding to a *Z* configuration, previously reported by Bruno et al [38]. This signal is outstanding for the product identification. Additionally, a phenol test with $FeCl_3$ was conducted to identify the final compounds. The compounds were obtained through a linear synthesis of five steps which were easy to obtain and were of a low structural complexity.

3.2. In vitro

3.2.1. PTP-1B inhibition assay

The final compounds **1** and **2** were tested as PTP-1B inhibitors at 20 μM. We found that compound **1** and **2** decrease the enzyme activity up to 85% and 50%, respectively. Taking into account these results, we have performed an additional concentration-response test in order to calculate the IC_{50} for the most active inhibitor, namely the compound **1** (Table 1).

Table 1
Ki value and inhibition type of compound **1** and **2**.

Compound	K_i (μM)	α	Inhibition type
1	3.7 ± 0.5	–	Non-competitive inhibition
2	3.5 ± 0.4	3.7	Mixed-type non-competitive inhibition

For this purpose, we studied the PTP-1B catalyzed hydrolysis of *p*-nitrophenyl phosphate by using different concentrations of compound **1**, measuring the time-course of *p*-nitrophenol release at 400 nm. We found that initial rates decrease with increasing inhibitor concentrations; therefore, its IC_{50} value was determined (Fig. 1). We found that compound **1** had an IC_{50} of 9.6 ± 0.5 μM.

Moreover, to define the action mechanism of compounds **1** and **2**, further assays were carried out. For each compound, we measured the initial hydrolysis rate using different substrate concentrations, and increasing inhibitor concentrations. The data that has been obtained were analysed by the double reciprocal plot (Fig. 2A, B). We found that experimental data that had been obtained with compound **1** describes straight lines intersecting from one another in a point on the x-axis, in the left quadrant. Moreover, we found that Vmax decreases in the presence of the inhibitor, but the Km value is not influenced. Based on the above results, we can conclude that compound **1** behaves as a non-competitive inhibitor (see Scheme 2A). Fig. 2B shows the double

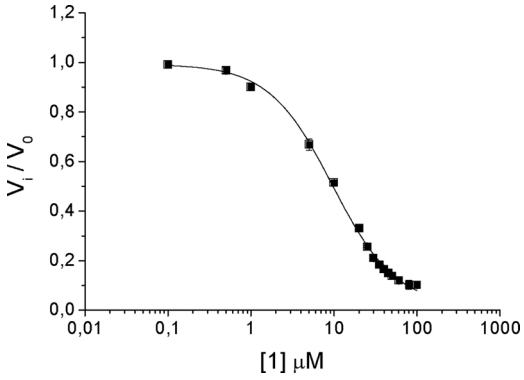

Fig. 1. The IC_{50} value was determined by plotting the relative activity of PTP-1B vs compound **1** concentration. Fifteen different inhibitor concentrations were used. All tests were performed in triplicate. The data represent the means ± S.E.M.

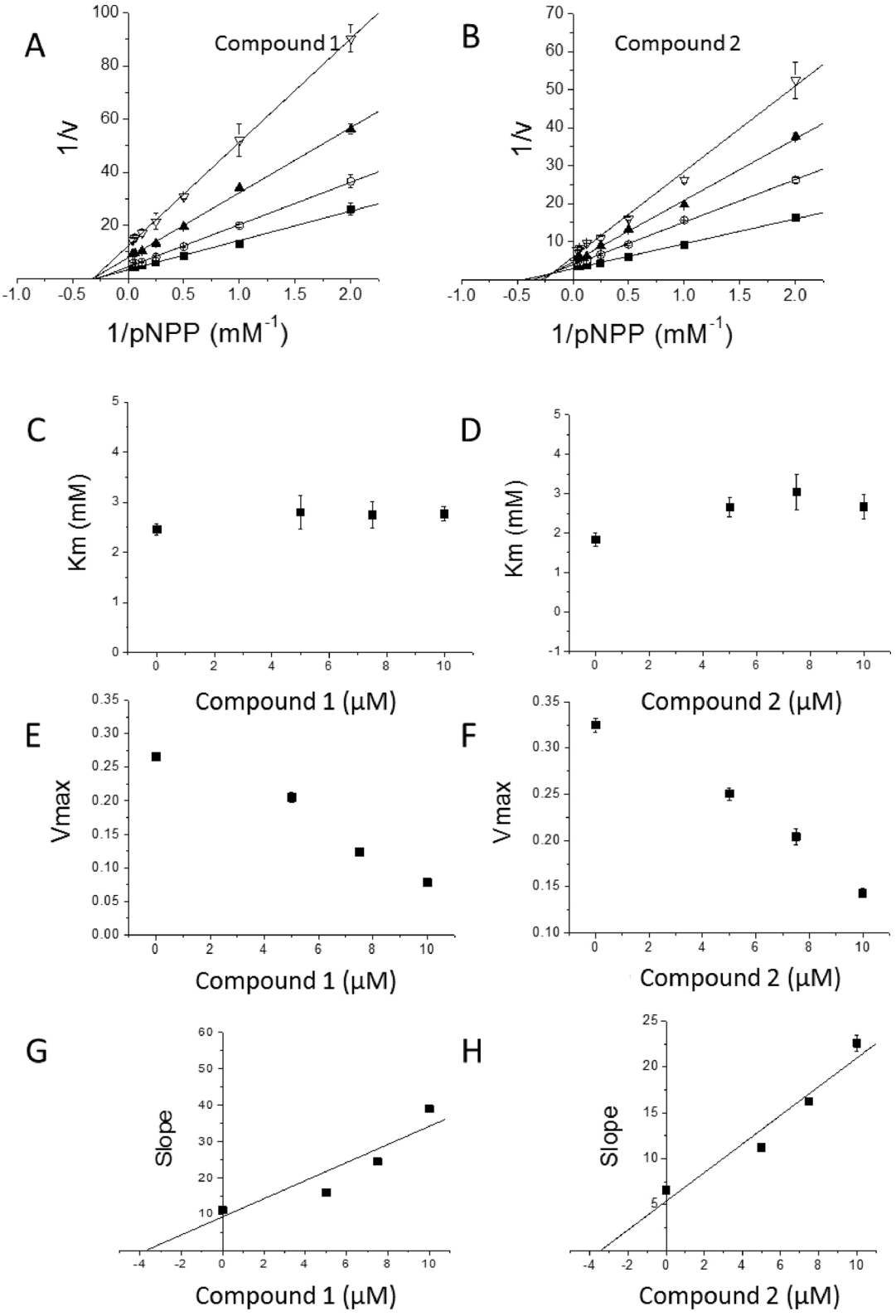

$$Slope = \frac{Km}{Vmax \times Ki}[I] + \frac{Km}{Vmax} \qquad \text{eq1}$$

$$Intercept = \frac{1}{Vmax \times Ki}[I] + \frac{1}{Vmax} \qquad \text{eq2}$$

Fig. 2. Double reciprocal plot (1/v versus 1/[S]). The inhibitor concentrations were the following: without inhibitor, ■; 5 µM, ○; 7.5 µM, ▲; 10 µM, ▼ to compound **1** (A) and without inhibitor ■; 7.5 µM, ○; 15 µM, ▲; 25 µM, ▼ to compounds **2** (B). All assays were performed in triplicate. The data reported in the graph, represent the means ± S.E.M. Dependence of mains kinetic parameters K_m and V_{max} from the concentration of compound **1** and **2** (C–F). Determination of Ki value: the slope values calculate by linear fitting in Figs. 2G-H were plotted versus compounds **1** and **2** concentrations. Fitting of data was carried out using Eqs. (1), and (2). The parameter α was calculate using Eq. (3).

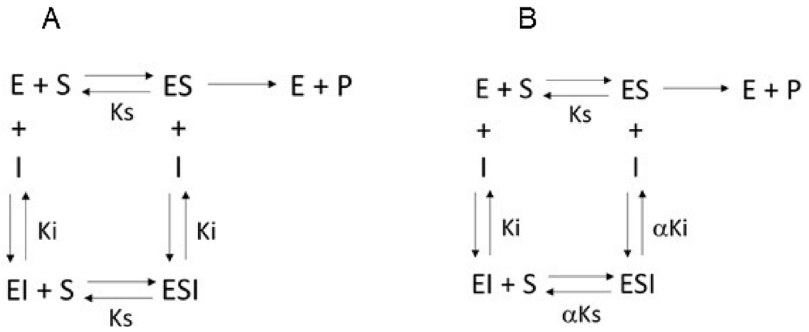

Scheme 2. A, non-competitive inhibition; B, Mixed-type non-competitive inhibition. E, free enzyme; ES enzyme-substrate complex; EI, enzyme-inhibitor complex; ESI, enzyme-substrate-inhibitor complex; Ks, enzyme substrate complex dissociation constant; Ki, enzyme-inhibitor complex dissociation constant; α > 1.

reciprocal plot obtained from compound **2**. We can observe that the straight lines that have been obtained by fitting experimental data intersect from one another in a point on the left quadrant. Moreover, both Km and Vmax values are affected by inhibitor (Km increases and Vmax decreases, respectively). Together, these evidences suggested that compound **2** behaved as a mixed-type non-competitive inhibitor (see Scheme 2B) Ki and α values were determined using the Eq. (1) (for compound **1**), and Eqs. (2) and (3) (for compound **2**).

$$Slope = \frac{Km}{Vmax} \times \left(\frac{[I]}{Ki}\right) + \frac{Km}{Vmax} \quad (1)$$

$$Slope = \frac{Km}{Vmax \times Ki}[I] + \frac{Km}{Vmax} \quad (2)$$

$$Intercept = \frac{1}{Vmax \times Ki}[I] + \frac{1}{Vmax} \quad (3)$$

3.3. In vivo

3.3.1. Antihyperglycemic activity

According to the stages of development and search for new bioactive compounds, the most active molecule on PTP-1B inhibition assay was evaluated for *in vivo* antihyperglycemic activity using a rat model of non-insulin-dependent diabetes mellitus (NIDDM). Compound **1** was found to be the most effective inhibitor of human PTP-1B. Glibenclamide was taken as the positive control. The antihyperglycemic activity was determined using a 50 mg/kg single dose. Compound **1** demonstrated a modest variation of glycaemia, decreasing up to 37% at 7 h post-administration. Compound **1** showed a similar percentage of variation than glibenclamide which was observed at 7 h of post-intragastric administration (Table 2). Finally, several 2-aminobenzothiazoles have been tested as antidiabetic compounds with promising results [39,40]. This inhibitory effect on the enzyme causes a prolonged effect of insulin since the receptor is sensitized to the action of the same insulin, which makes the small amount of insulin more efficient in this murine model.

3.4. In silico

3.4.1. Molecular docking of compounds 1 and 2

In effort to explain the best activity showed by compound **1**, we performed a molecular docking on a PTP-1B structure in order to find the possible binding mode. The molecules were docked with a crystallographic structure of a human PTP-1B (PDB code 1C83, [41]) covering two binding sites reported by Puius [42]. Compounds **1** and **2** were docked showing good affinities with free binding energy of −8.94 Kcal/mol and −8.04 Kcal/mol, respectively. Fig. 3 shows the binding mode of **1** which has conserved two interactions with the most important residues that were involved into a catalytic triad of PTP-1B (Asp181 and Arg221) and other H-bonds with Arg47 and Asp48 residues. Moreover, compound **2** also has significant interactions with Asp 181, Arg221 and Tyr46 (Fig. 4), both had interactions at least with one residue of site B, however, the flexible spacer in compound **1** gives it a better bond strength. As compared to the crystallographic ligand, compound **1** and **2** lack of numerous important hydrogen bonds with Lys120, Ser216, Ala217 and Gly220. Interestingly, two H-bonds were conserved with two residues, which are catalytic residues. In both cases the phenol moiety was oriented towards a catalytic pocket, but the other portion of the molecule is directed to the exposed surface of the catalytic site. Also, the benzazole fragment can be strengthening the interaction with this extended site. Although benzimidazole has one more hydrogen bond donor than the benzothiazole, it seems that the space between thiazolidine-2,4-dione core and benzazole favored the enzyme inhibition when the distance between the two cores are longer. This proposes that the binding site could be located in site B (extended site) near to the catalytic site A [43]. These results strengthen the previous enzymatic tests and could explain or indicate that compound **1** occupies the binding site and thereby blocks the enzyme activity by obstruction of the catalytic site and its interaction with two catalytic residues. Figs. 3 and 4 depicts the corresponding amino acid residues at 4.5 Å in a 2D interaction map that was generated with the Molecular Operating Environment (MOE) software package [44].

3.4.2. ADMET properties calculation

Pharmacokinetic parameters of compounds 1 and 2 (Table 3) were calculated using the admetSAR web server [45]. This information was required to optimize the pharmacodynamic response and extent of

Table 2
Effect of a single dose of **1** (50 mg/Kg; intragastric, n = 5) in streptozotocin-nicotinamide-induced diabetes rat model.

Compd	Dose (mg/Kg)	Percentage of variation of glycemia ± SEM (mg/dL)				
		Zero hour	First hour	Third hour	Fifth hour	Seventh hour
1	50	0.0 ± 0.0	16.0 ± 3.5	−1 ± 2.2	−11.0 ± 7.5	−34.0 ± 4.4*
Gli	5	0.0 ± 0.0	−20.4 ± 8.2*	−36.3 ± 7.5*	−37.5 ± 0.5*	−43.6 ± 9.9*

Vehicle: Isotonic saline solution. *p < 0.05 versus ISS group. The negative value indicates drecrese in glycemia. Gli, Glibenclamide.

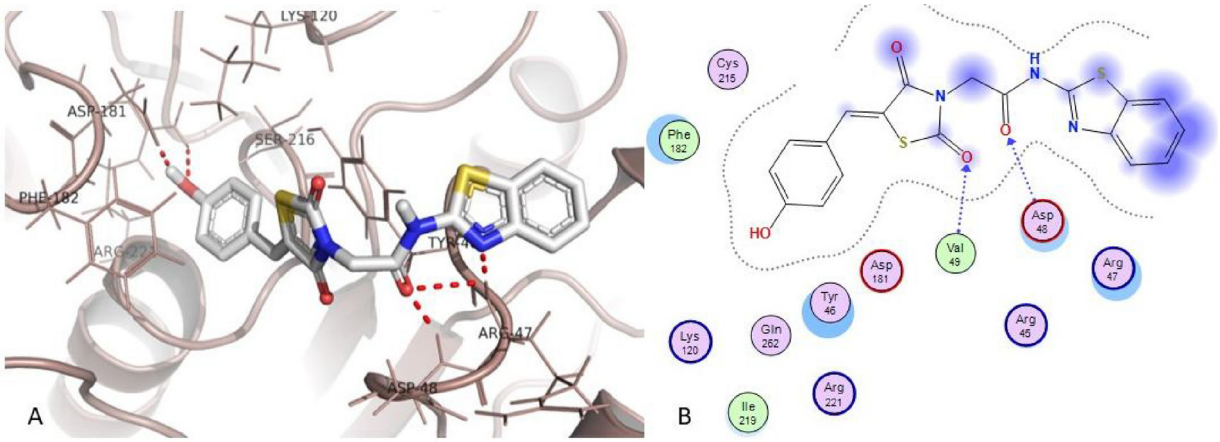

Fig. 3. The proposed binding mode of compound **1** with the best free binding energy (-8.94 Kcal/mol) in the active site of PTP-1B. A) Compound 1 was colored by atom types (carbon atoms colored gray) and hydrogen bond network is denoted as red dashed lines. Five polar contacts were detected with Val49, Arg221, Asp181, Arg47 and Asp48 residues. B) 2D interaction map of **1** docked into the PTP-1B binding pocket.

availability as a function in the route of administration. The results obtained from the BBB (Blood-Brain Barrier) penetrability were agreeable for both compounds, which showed an intermediate to low probability of crossing the BBB reducing the possible toxicity in the central nervous system. We also found that the two tested compounds could be absorbed by the human intestine, that could allow them to reach the site of action, nevertheless, both showed a poor penetration to Caco-2.

On the other hand, the tested compounds did not seem to be potential substrates or inhibitors for the P-glycoprotein (P-gp) which effluxes drugs and various compounds and this is considered as a multidrug resistant target. In contrast, there are several cytochrome P450 isoforms and the inhibition of cytochrome P450 isoforms might cause drug-drug interactions in which co-administered drugs are unsuccessful to metabolize and increase the amount of drugs to toxic levels [46]. Nevertheless, more than a few of cytochrome P450 isoforms could be inhibited by one or more of the tested compounds. Fortunately, we were able to find compounds that did not exhibit inhibition over all isoforms but the compounds showed a preference to isoform CYP 2C9. Both compounds did not show any carcinogenic and mutagenic effect and genotoxicity in the Ames test. Finally, the compounds demonstrated to be safe with LD_{50} values greater than 500 mg/kg but less than 2000 mg/kg (Category III).

4. Conclusions

We have described the synthesis of two molecules that were easily obtainable and used *in combo* evaluations (*in vitro*, *in silico* and *in vivo* assays). The enzymatic activity results suggested that the molecule with amide spacer group (compound **1**) induces better activity than compound **2**, which lacks this portion. Interestingly, compound **1** showed an *in vivo* antidiabetic activity. The correlation between *in vitro* and *in vivo* assays indicates that compounds **1** and **2** have potential characteristics that improve their affinity. On the other hand, the potency between compounds was dramatically improved by the addition of a spacer, which gives the molecule the ability to take an enhanced conformation in the recognition site in enzymes. Furthermore, the introduction of privileged heterocyclic scaffold as benzothiazole and benzimidazole provides acceptable drug-like properties with an easy modification that can help us to obtain ligands with requirements for better interaction. Finally, the molecular docking has revealed the importance of an H-bond acceptor that improves the interaction between ligand and binding site residues. In this case, that was the phenol fragment of the molecule. The groundwork for the future design of specific compounds with better affinity and selectivity is to find ligands that can interact with two PTP-1B binding sites (A and B). These considerations could be taken into account to design new compounds. Finally, the two compounds have satisfactory calculated

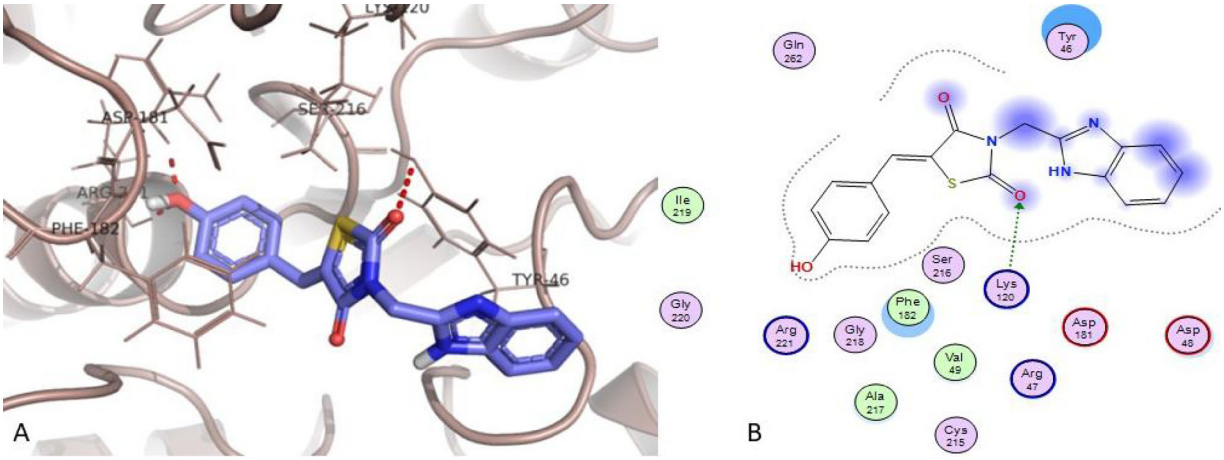

Fig. 4. The proposed binding mode of compound 2 with the free binding energy of −8.04 Kcal/mol. A) Compound 2 was colored by atom types (carbon atoms colored blue) and hydrogen bond network is denoted as red dashed lines. Three polar contacts were detected: two H-bonds with Arg221, Lys 120 andTyr46 residues. B) 2D interaction map of **2** docked into the PTP-1B binding pocket.

Table 3
ADMET properties calculated for compounds **1** and **2**.

Model	Result	Probability	
		Compound 1	Compound 2
Absorption			
Blood-Brain Barrier	BBB	(+) 0.5277	(-) 0.8861
Human Intestinal Absorption	HIA+	0.9382	0.9970
Caco-2 Permeability	Caco2-	0.6734	0.5812
P-glycoprotein Substrate	Substrate	0.5959	0.6483
P-glycoprotein Inhibitor	Non-inhibitor	0.8671	0.9083
	Non-inhibitor	0.7756	0.8683
Renal Organic Cation Transporter	Non-inhibitor	0.8293	0.7473
Metabolism			
CYP450 2C9 Substrate	Non-substrate	0.7787	0.8153
CYP450 2D6 Substrate	Non-substrate	0.8284	0.8033
CYP450 3A4 Substrate	Non-substrate	0.5542	0.6162
CYP450 1A2 Inhibitor	Non-inhibitor	0.8293	0.5000
CYP450 2C9 Inhibitor	Inhibitor	0.7122	0.6183
CYP450 2D6 Inhibitor	Non-inhibitor	0.7533	0.6962
CYP450 2C19 Inhibitor	Non-inhibitor	0.6818	0.5529
CYP450 3A4 Inhibitor	Non-inhibitor	0.9012	0.5199
CYP Inhibitory Promiscuity	Low CYP Inh Promiscuity	0.5269	0.6999
Toxicity			
Human Ether-a-go-go-Related Gene Inhibition	Weak inhibitor	0.8564	0.9355
	Non-inhibitor	0.7490	0.7489
AMES Toxicity	Non AMES toxic	0.6880	0.6418
Carcinogens	Non-carcinogens	0.8080	0.8382
Cacinogenicity	Non-required	0.5078	0.5065
Acute Oral Toxicity	III	0.6060	0.6687

Model	Units	Probability	
		Compound 1	Compound 2
ADMET predicted Profile-Regression			
Aqueous solubility	LogS	−3.4327	−3.6185
Caco-2 Permeability	LogPapp, cm/s	0.6929	1.1082
Rat Acute Toxicity	LD50, mol/kg	2.3240	2.5775
Fish Toxicity	pLC50, mg/L	1.1345	1.2586
Tetrahymena pyriformis Toxicity	pIGC50, ug/L	0.4939	0.5023

pharmacokinetics parameters values which make promising molecules that allow us to continue their revision.

Conflict of interests

The authors declare that there is no conflict of interests regarding to the publication of this paper.

Acknowledgements

This work was supported in part by the National Council of Science and Technology (CONACyT), grant 253814. The authors would like to thank the Facultad de Farmacia (UAEM) internal grant for providing the research materials for this study, and Lucia Aldana Navarro for her grammatical review.

References

[1] R. Lesyk, B. Zimenkovsky, D. Atamanyuk, F. Jensen, K. Kiec-Kononowicz, Gzella A, Anticancer thiopyrano[2,3-*d*][1,3]thiazol-2-ones with norbornane moiety. Synthesis, cytotoxicity, physico-chemical properties, and computational studies, Bioorg. Med. Chem. 14 (2006) 5230–5240.
[2] D. Havrylyuk, B. Zimenkovsky, O. Vasylenko, L. Zaprutko, A. Gzella, R. Lesyk, Synthesis of novel thiazolone-based compounds containing pyrazoline moiety and evaluation of their anticancer activity, Eur. J. Med. Chem. 44 (2009) 1396–1404.
[3] B. Kaminskyy, B. Zimenkovsky, R. Lesyk, Synthesis and *in vitro* anticancer activity of 2,4-azolidinedione-acetic acids derivatives, Eur. J. Med. Chem. 44 (2009) 3627–3636.
[4] R. Ottanà, R. Maccari, M.L. Barreca, G. Bruno, A. Rotondo, A. Rossi, G. Chiricosta, R. Di Paola, L. Sautebin, S. Cuzzocrea, M.G. Vigorita, 5-Arylidene-2-imino-4-thiazolidinones: design and synthesis of novel anti-inflammatory agents, Bioorg. Med. Chem. 13 (2005) 4243–4252.
[5] A.D. Taranalli, A.R. Bhat, S. Srinivas, E. Saravanan, Antiinflammatory, Analgesic and Antipyretic Activity of Certain Thiazolidinones, J. Pharm. Sci. 70 (2008) 159–164.
[6] A. Deep, S. Jain, P.C. Sharma, Synthesis and anti-inflammatory activity of some novel biphenyl-4-carboxylic acid 5-(arylidene)-2-(aryl)-4-oxothiazolidin-3-yl amides, Act. Pol. Pharm. 67 (2010) 63–67.
[7] C.J. Andres, J.J. Bronson, S.V. D'Andrea, M.S. Deshpande, P.J. Falk, K.A. Grant-Young, W.E. Harte, H.T. Ho, P.F. Misco, J.G. Robertson, D. Stock, Y. Sun, A.W. Walsh, 4-Thiazolidinones: novel inhibitors of the bacterial enzyme MurB, Bioorg. Med. Chem. Lett. 10 (2000) 715–717.
[8] P. Vicini, A. Geronikaki, K. Anastasia, M. Incerti, F. Zani, Synthesis and antimicrobial activity of novel 2-thiazolylimino-5-arylidene-4-thiazolidinones, Bioorg. Med. Chem. 14 (2006) 3859–3864.
[9] B. Samir, K. Wesam, A.F. Ahmed, Synthesis and antimicrobial evaluation of some new thiazole, thiazolidinone and thiazoline derivatives starting from 1-chloro-3,4-dihydronaphthalene-2-carboxaldehyde, Eur. J. Med. Chem. 42 (2007) 948–954.
[10] I.M. Silva, J. Silva Filho, J.B.Gomes da Silva Santiago, M.S. Egito, C.A. Souza, F.L. Gouveia, R.F. Ximenes, F.X. Fonseca Ribeiro de Sena, A.R. de Faria, D.J. Brondani, J.F. Cavalcanti de Albuquerque, Synthesis and antimicrobial activities of 5-Arylidene-thiazolidine-2,4-dione derivatives, Bio. Med. Res. Int. 2014 (2014) 1–8.
[11] A.A. El-Barbary, A.I. Khodair, E.B. Pedersen, C. Nielsen, Synthesis and Evaluation of Antiviral Activity of 2'-Deoxyuridines with 5-Methylene-2-thiohydantoin Substituents in the 5-position, Monatsh. Chem. 125 (1994) 593–598.
[12] Y. Liu, F. Jing, Y. Xu, Y. Xie, F. Shi, H. Fang, M. Li, W. Xu, Design, synthesis and biological activity of thiazolidine-4-carboxylic acid derivatives as novel influenza neuraminidase inhibitors, Bioorg. Med. Chem. 19 (2011) 2342–2348.
[13] P.G. Marshall, D.K. Vallance, Anticonvulsant activity; derivatives of succinimide, glutarimide, thiazolidinedione and methanol, and some miscellaneous compounds, J. Pharm. Pharmacol. 6 (1954) 740–746.
[14] E. Rydzik, A. Szadowska, A. Kaminska, Synteza benzylideno wych pochodnych 3-o-, 3-m- i 3-p-chlorofenylohydantoiny i badanie ich właściwości przeciwdrgawkowych. [[Synthesis of benzylidene derivatives of 3-o, 3-m and 3-p-chlorophenylhydantoin and the study of their anticonvulsant action]], Acta Pol. Pharm. 41 (1984) 459–464.
[15] H.L. Liu, Z.C. Li, T. Anthonsen, Synthesis and fungicidal activity of 2-Imino-3-(4-arylthiazol-2-yl)-thiazolidin-4-ones and their 5-Arylidene derivatives, Molecules 5

(2000) 1055–1061.
[16] Y.M. Ha, Y.J. Park, J.A. Kim, D. Park, J.Y. Park, H.J. Lee, J.Y. Lee, H.R. Moon, H.Y. Chung, Design and synthesis of 5-(substitutedbenzylidene)thiazolidine-2,4-dione derivatives as novel tyrosinase inhibitors, Eur. J. Med. Chem. 49 (2012) 245–252.
[17] S. Hidalgo-Figueroa, J.J. Ramírez-Espinosa, S. Estrada-Soto, J.C. Almanza-Pérez, R. Román-Ramos, F.J. Alarcón-Aguilar, J.V. Hernández-Rosado, H. Moreno-Díaz, D. Díaz-Coutiño, G. Navarrete-Vázquez, Discovery of Thiazolidine-2,4-Dione/Biphenylcarbonitrile hybrid as dual PPAR α/γ modulator with antidiabetic effect: *in vitro*, *in Silico* and *in vivo* approaches, Chem. Biol. Drug Des. 81 (2013) 474–483.
[18] G. Navarrete-Vázquez, H. Torres-Gómez, S. Hidalgo-Figueroa, J.J. Ramírez-Espinosa, S. Estrada-Soto, J.L. Medina-Franco, I. León-Rivera, F.J. Alarcón-Aguilar, J.C. Almanza-Pérez, Synthesis, *in vitro* and *in silico* studies of a PPARγ and GLUT-4 modulator with hypoglycemic effect, Bioorg. Med. Chem. Letts. 24 (2014) 4575–4579.
[19] R. Maccari, P. Paoli, R. Ottanà, M. Jacomelli, R. Ciurleo, G. Manao, T. Steindl, T. Langer, M.G. Vigorita, G. Camici, 5-Arylidene-2,4-thiazolidinediones as inhibitors of protein tyrosine phosphatases, Bioorg. Med. Chem. 15 (2007) 5137–5149.
[20] R. Ottanà, R. Maccari, R. Ciurleo, P. Paoli, M. Jacomelli, G. Manao, G. Camici, C. Laggner, T. Langer, 5-Arylidene-2-phenylimino-4-thiazolidinones as PTP1B and LMW-PTP inhibitors, Bioorg. Med. Chem. 17 (2009) 1928–1937.
[21] R. Ottanà, R. Maccari, R. Amuso, G. Wolber, D. Schuster, S. Herdlinger, G. Manao, G. Camici, P. Paoli, New 4-[(5-arylidene-2-arylimino-4-oxo-3 thiazolidinyl)methyl] benzoic acids active as protein tyrosine phosphatase inhibitors endowed with insulinomimetic effect on mouse C2C12 skeletal muscle cells, Eur. J. Med. Chem. 53 (2012) 332–343.
[22] R. Ottanà, R. Maccari, J. Mortier, A. Caselli, S. Amuso, G. Camici, A. Rotondo, G. Wolber, P. Paoli, Synthesis, biological activity and structure-activity relationships of new benzoic acid-based protein tyrosine phosphatase inhibitors endowed with insulinomimetic effects in mouse C2C12 skeletal muscle cells, Eur. J. Med. Chem. 71 (2014) 112–127.
[23] R. Ottanà, P. Paoli, A. Naß, G. Lori, V. Cardile, I. Adornato, A. Rotondo, A.C.E. Graziano, G. Wolber, R. Maccari, Discovery of 4-[(5-arylidene-4-oxothiazolidin-3-yl)methyl]benzoic acid derivatives active as novel potent allosteric inhibitors of protein tyrosine phosphatase 1B: in silico studies and in vitro evaluation as insulinomimetic and anti-inflammatory agents, Eur. J. Med. Chem. 127 (2017) 840–858.
[24] K.A. Kenner, E. Anyanwu, J.M. Olefsky, J. Kusari, Protein-tyrosine phosphatase 1B is a negative regulator of insulin- and insulin-like growth Factor-I-stimulated signaling, J. Biol. Chem. 271 (1996) 19810–19816.
[25] B.L. Seely, P.A. Staubs, D.R. Reichart, P. Berhanu, K.L. Milarski, A.R. Saltiel, J. Kusari, J.M. Olefsky, Protein tyrosine phosphatase 1B interacts with the activated insulin receptor, Diabetes 45 (1996) 1379–1385.
[26] D. Bandyopadhyay, A. Kusari, K.A. Kenner, F. Liu, J. Chernoff, T.A. Gustafson, J. Kusari, Protein-tyrosine phosphatase 1B complexes with the insulin receptor in vivo and is tyrosine-phosphorylated in the presence of insulin, J. Biol. Chem. 272 (1997) 1639–1645.
[27] J.C. Byon, A.B. Kusari, J. Kusari, Protein-tyrosine phosphatase-1B acts as a negative regulator of insulin signal transduction, Mol. Cell. Biochem. 182 (1998) 101–108.
[28] S. Dadke, A. Kusari, J. Kusari, Phosphorylation and activation of protein tyrosine phosphatase (PTP) 1B by insulin receptor, Mol. Cell. Biochem. 221 (2001) 147–154.
[29] K.L. Guan, J.E. Dixon, Evidence for protein-tyrosine-phosphatase catalysis proceeding via a cysteine-phosphate intermediate, J. Biol. Chem. 266 (1991) 17026–17030.
[30] L. Bialy, H. Waldmann, Inhibitors of Protein Tyrosine Phosphatases: Next-Generation Drugs? Angew. Chem. Int. 44 (2005) 3814–3839.
[31] U.K. Laemmli, Cleavage of structural proteins during the assembly of the head of bacteriophage T4, Nature 227 (1979) 680–685.
[32] P. Paoli, A. Modesti, F. Magherini, T. Gamberi, A. Caselli, G. Manao, G. Raugei, G. Camici, G. Ramponi, Site-directed mutagenesis of two aromatic residues lining the active site pocket of the yeast Ltp1, Biochim. Biophys. Acta 1770 (2007) 753–762.
[33] M. Torres-Piedra, R. Ortiz-Andrade, R. Villalobos-Molina, N. Singh, J.L. Medina-Franco, S.P. Webster, M. Binnie, G. Navarrete-Vázquez, S. Estrada-Soto, A comparative study of flavonoid analogues on streptozotocin-nicotinamide induced diabetic rats: quercetin as a potential antidiabetic agent acting via 11b-hydroxysteroid dehydrogenase type 1 inhibition, Eur. J. Med. Chem. 45 (2010) 2606–2612.
[34] S. Hidalgo-Figueroa, G. Navarrete-Vázquez, S. Estrada-Soto, D. Giles-Rivas, F.J. Alarcón-Aguilar, I. León-Rivera, A. Giacoman-Martínez, E. Miranda Pérez, J.C. Almanza-Pérez, Discovery of new dual PPARg-GPR40 agonists with robust antidiabetic activity: Design, synthesis and in combo drug evaluation, Biomed. Pharmacother. 90 (2017) 53–61.
[35] Avogadro: an open-source molecular builder and visualization tool. Version 1.2.0. http://avogadro.cc/.
[36] M.D. Hanwell, D.E. Curtis, D.C. Lonie, T. Vandermeersch, E. Zurek, G.R. Hutchison, Avogadro: an advanced semantic chemical editor, visualization, and analysis platform, J. Cheminform. 4 (2012) 17.
[37] G.M. Morris, R. Huey, W. Lindstrom, M.F. Sanner, R.K. Belew, D.S. Goodsell, A.J. Olson, J. Comp. Chem. 16 (2009) 2785–2791.
[38] G. Bruno, L. Constantino, C. Curinga, R. Maccari, F. Monforte, F. Nicolo, R. Ottana, M.G. Vigorita, Synthesis and aldose reductase inhibitory activity of 5-arylidene-2,4-thiazolidinediones, Bioorg. Med. Chem. 10 (2002) 1077–1084.
[39] G. Navarrete-Vázquez, P. Paoli, I. León-Rivera, R. Villalobos-Molina, J.L. Medina-Franco, R. Ortiz-Andrade, S. Estrada-Soto, G. Camici, D. Diaz-Coutiño, I. Gallardo-Ortiz, K. Martinez-Mayorga, H. Moreno-Díaz, Synthesis, *in vitro* and computational studies of protein tyrosine phosphatase 1B inhibition of a small library of 2-arylsulfonylaminobenzothiazoles with antihyperglycemic activity, Bioorg. Med. Chem. 7 (2009) 3332–3341.
[40] G. Navarrete-Vazquez, M. Ramírez-Martínez, S. Estrada-Soto, C. Nava-Zuazo, P. Paoli, G. Camici, J. Escalante-García, J.L. Medina-Franco, F. López-Vallejo, R. Ortiz-Andrade, Synthesis, in vitro and in silico screening of ethyl 2-(6-substituted benzo[d]thiazol-2-ylamino)-2-oxoacetates as protein-tyrosine phosphatase 1B inhibitors, Eur. J. Med. Chem. 53 (2012) 346–355.
[41] H.S. Andersen, L.F. Iversen, C.B. Jeppesen, S. Branner, K. Norris, H.B. Rasmussen, K.B. Moller, N.P. Moller, 2-(oxalylamino)-benzoic acid is a general, competitive inhibitor of protein-tyrosine phosphatases, J. Biol. Chem. 275 (2000) 7101–7108.
[42] Y.A. Puius, Y. Zhao, M. Sulliovan, D.S. Lawrence, S.C. Almo, Z. Zhang, Identification of a second aryl phosphatebinding site in protein-tyrosine phosphatase 1B: a paradigm for inhibitor design, Proc. Natl. Acad. Sci. U.S.A. 94 (1997) 13420–13425.
[43] R. Guzmán-Ávila, V. Flores-Morales, P. Paoli, G. Camici, J.J. Ramírez-Espinosa, L. Cerón-Romero, G. Navarrete-Vázquez, S. Hidalgo-Figueroa, M. Yolanda Rios, R. Villalobos-Molina, S. Estrada-Soto, Ursolic acid derivatives as potential antidiabetic agents: in vitro, in vivo, and in silico studies, Drug Dev. Res. 79 (2018) 70–80.
[44] Molecular Operating Environment (MOE), 2016.08, Chemical Computing group ULC, 1010 Sherbooke St. West, Site #910, Montreal, QC, Canada, H3A 2R7, 2018http://www.chemcomp.com.
[45] F. Cheng, W. Li, Y. Zhou, J. Shen, Z. Wu, G.W. Liu, P. Lee, Y. Tang, AdmetSAR: a comprehensive source and free tool for evaluating chemical ADMET properties, J. Chem. Inf. Model. 52 (2012) 3099–3105.
[46] B. Colín-Lozano, S. Estrada-Soto, F. Chávez-Silva, A. Gutiérrez-Hernández, L. Cerón-Romero, A. Giacoman-Martínez, J.C. Almanza-Pérez, E. Hernández-Núñez, Z. Wang, X. Xie, M. Cappiello, F. Balestri, U. Mura, G. Navarrete-Vazquez, Synthesis and in combo antidiabetic bioevaluation of multitarget phenylpropanoic acids, Molecules 23 (2018) 340.